



## Application of $C_{14}/SiO_2-Fe_3O_4$ and $AC-Fe_3O_4$ nanocomposite for U(VI) removal

Zohreh Akbari-Jonoush<sup>a</sup>, Simin Naseri<sup>a,b</sup>, Mahdi Farzadkia<sup>c,\*</sup>,  
Hamid-Reza Mohajerani<sup>d</sup>, Mehdi Shirzad-Siboni<sup>c,\*</sup>, Jae-Kyu Yang<sup>e</sup>

<sup>a</sup>Department of Environmental Health Engineering, School of Public Health, Tehran University of Medical Sciences, Tehran, Iran, emails: [z\\_akbari1229@yahoo.com](mailto:z_akbari1229@yahoo.com) (Z. Akbari-Jonoush), [naserise@tums.ac.ir](mailto:naserise@tums.ac.ir) (S. Naseri)

<sup>b</sup>Center for Water Quality Research (CWOR), Institute for Environmental Research (IER), Tehran University of Medical Sciences, Tehran, Iran

<sup>c</sup>Department of Environmental Health Engineering, School of Public Health, Iran University of Medical Sciences, Tehran, Iran, Tel. +98 9122588677; Fax: +98 2188607939; email: [mahdifarzadkia@gmail.com](mailto:mahdifarzadkia@gmail.com) (M. Farzadkia), Tel. +98 9112346428; Fax: +98 2188607939; emails: [mshirzadsiboni@yahoo.com](mailto:mshirzadsiboni@yahoo.com), [shirzad.m@iums.ac.ir](mailto:shirzad.m@iums.ac.ir) (M. Shirzad-Siboni)

<sup>d</sup>Iran Radioactive Waste Management Company, Atomic Energy Organization of Iran, Tehran, Iran, email: [hmohajerani@aeoi.org.ir](mailto:hmohajerani@aeoi.org.ir)

<sup>e</sup>Division of General Education, Kwangwoon University, Seoul 139-701, Korea, email: [jkyang@kw.ac.kr](mailto:jkyang@kw.ac.kr)

Received 13 May 2015; Accepted 3 December 2015

---

### ABSTRACT

In this study,  $C_{14}/SiO_2-Fe_3O_4$  and  $AC-Fe_3O_4$  nanocomposite synthesized by co-precipitation method were used as adsorbents for the removal of U(VI) from aqueous solutions. The main compositions of  $AC-Fe_3O_4$  and  $C_{14}/SiO_2-Fe_3O_4$  were characterized by Fourier transform infrared spectroscopy, X-ray diffraction, and scanning electron microscopy. The removal efficiency of U(VI) was studied as a function of pH, contact time, ionic strength, temperature, adsorbent dose, initial U(VI) concentration, and initial benzamide concentration. Maximum adsorption of U(VI) was obtained at pH 6. The removal of U(VI) reached an equilibrium within 30 min by  $C_{14}/SiO_2-Fe_3O_4$  and 90 min by  $AC-Fe_3O_4$ , respectively. Removal efficiency of U(VI) by both adsorbents was decreased with increasing ionic strength and initial U(VI) concentration, but was increased with increasing temperature and adsorbent dosage. Kinetic study revealed that the pseudo-second order model well described the adsorption of U(VI) onto two adsorbents. When adsorption data was analyzed by both Langmuir and Freundlich adsorption isotherms, it was better described by the Langmuir model. The maximum adsorption of U(VI) was 16.29 and 15.87 mg/g by  $C_{14}/SiO_2-Fe_3O_4$  and  $AC-Fe_3O_4$  nanocomposite, respectively. The thermodynamic parameters of the adsorption process indicated that adsorption occurred through endothermic process. Overall, this work shows that  $C_{14}/SiO_2-Fe_3O_4$  is a more effective adsorbent than  $AC-Fe_3O_4$  for the removal of low concentration of U(VI).

*Keywords:* Adsorption; U(VI);  $C_{14}/SiO_2-Fe_3O_4$ ;  $AC-Fe_3O_4$ ; Kinetics and isotherm models

---

\*Corresponding authors.

## 1. Introduction

In recent years, contamination of surface and ground waters is regarded as one of the most important environmental issues. Radionuclides having high toxicity and non-biodegradability cause several problems in environmental systems and public health [1–3]. Generally, uranium concentration in natural environment is very low [4,5]. But artificial use of uranium as nuclear fuel [2,6–8] is serious concern in environment and human health. Under aerobic condition, uranium exists predominantly as a hexavalent species [9,10], which is soluble and mobile [11–13]. So uranium contaminated in soils can be transferred to surface and groundwater. The inhalation and ingestion of uranium can cause irreversible lungs and kidney damage or even death [12,14,15] due to its long half-life as well as chemical and radiological toxicity [16,17]. Recently, a few studies have shown that the central nervous system is sensitive to uranium because it crosses the blood–brain barrier and accumulates in brain [18]. One of the sources of uranium accumulation in human body is ingestion of contaminated drinking water [19]. Thus, united states environmental protection agency (US-EPA) and World Health Organization (WHO) established a maximum contaminant level (MCL) for uranium in drinking water as 30 and 9  $\mu\text{g/L}$ , respectively [20,21]. Due to the several problems mentioned above, finding a proper method for the treatment of water contaminated with uranium becomes an important research topic. Among several traditional methods such as adsorption, coagulation, precipitation, reverse osmosis, electrochemical treatments, ion exchange, membrane separation [2,22,23], adsorption is an effective method for the removal of moderate and low concentration of uranium due to its simplicity of design and operation, high capacity, and ease of regeneration [6,24–27]. In recent years, several kinds of adsorbents have been used for the removal of uranium. Among them, nano-sized adsorbents are more effective and attractive because of their high surface area to volume ratio and convenience in the modification of their surface functionality [28]. But separation of the nano-sized adsorbents is very difficult in practical application. Recently, many efforts have been devoted to synthesize super paramagnetic nanocomposites combined with iron oxide nanoparticles. These adsorbents can be easily separated by an external magnetic field without no costly process such as centrifugation or filtration [29,30]. Das et al. reported that  $\text{Fe}_3\text{O}_4$  nanoparticles had approximately 5 mg/g adsorption capacity of U(VI) [31]. Therefore, modification of chemical and physical properties of  $\text{Fe}_3\text{O}_4$  nanoparticles has much attention.  $\text{Fe}_3\text{O}_4$ – $\text{SiO}_2$

nanocomposite has an iron oxide core and a silica shell. Silica shell plays an important role in physical and chemical properties of the nanocomposite because it can prevent damage of physical and magnetic properties of the coated material [32] as well as aggregation of particles in solution [15]. There are several studies about modification of  $\text{Fe}_3\text{O}_4$ – $\text{SiO}_2$  nanocomposite. For example, Sha et al. and Wang et al. modified  $\text{Fe}_3\text{O}_4$ – $\text{SiO}_2$  nanocomposite by chlorodimethyl-*n*-octadecylsilan and (3-aminopropyl)trimethoxysilane (APTMS) [33,34]. Chang grafted hexadecyltrimethoxysilane (HTMOS) onto the surface of  $\text{Fe}_3\text{O}_4$ – $\text{SiO}_2$  nanocomposite [35]. Tan et al. used 1,6-hexanediamine for modification of  $\text{Fe}_3\text{O}_4$ – $\text{SiO}_2$  nanocomposite [1] and Ahangaran used vinyltriethoxysilane as a silane coupling agent for the modification of  $\text{Fe}_3\text{O}_4$ – $\text{SiO}_2$  nanocomposite [32]. Another way for increasing the adsorption capacity of  $\text{Fe}_3\text{O}_4$  nanoparticles is coating of them on the effective and economic adsorbents. Activated carbon is widely used in the treatment of various industrial effluents because it has a higher thermal and radiation resistance, better acid–base stability, high surface area, and porosity [36].

Hence, in this study,  $\text{Fe}_3\text{O}_4$ – $\text{SiO}_2$  nanocomposite modified by triethoxyoctylsilane ( $\text{C}_{14}/\text{SiO}_2$ – $\text{Fe}_3\text{O}_4$ ) and AC– $\text{Fe}_3\text{O}_4$  nanocomposite was used to remove U(VI) from aqueous solutions. Benzamide ( $\text{C}_7\text{H}_7\text{ON}$ ), which is a derivative of benzoic acid, was used as medium solution because it has donor atoms (N, O) that can form complexes with uranyl ions [16,37]. The adsorption behavior of these adsorbents toward U(VI) was investigated with respect to different experimental conditions such as initial solution pH, contact time, ionic strength, temperature, adsorbent dose, concentration of U(VI), and concentration of benzamide. The adsorption kinetics, isotherms, and thermodynamics were conducted to evaluate the adsorption capacity of  $\text{C}_{14}/\text{SiO}_2$ – $\text{Fe}_3\text{O}_4$  and AC– $\text{Fe}_3\text{O}_4$  nanocomposite.

## 2. Materials and methods

### 2.1. Chemicals

Triethoxyoctylsilane, tetraethylorthosilicate (98%), benzamide, pyridine, toluene, ethanol, arsenazo(III), ammonium solution, iron(II) chloride, iron(III) chloride (97%), zinc (99%), and activated carbon, which were of analytical grade, were purchased from Merck, Germany. The initial pH of solution was adjusted by the addition of 0.1 M NaOH or HCl and was measured by pH meter (HQ40d HACH, US). The experiments were carried out at constant temperature in a shaking incubator (Labcon, Afrika). Uranium stock solution (1,000 mg/L) was prepared by dissolving

appropriate amounts of  $C_4H_6O_6 \cdot 2H_2O$  with 99% purity (Merck, Germany) in distilled water.

## 2.2. Preparation of magnetic adsorbents

### 2.2.1. Synthesis of $C_{14}/SiO_2-Fe_3O_4$ nanocomposite

First,  $Fe_3O_4$  nanoparticles were synthesized by coprecipitation of  $Fe^{2+}$  and  $Fe^{3+}$  ions in an ammonia solution [38]. Typically, 8.48 g  $FeCl_3 \cdot 6H_2O$  and 2.25 g  $FeCl_2 \cdot 4H_2O$  were dissolved in 400-mL distilled water for 1 h at 80°C under  $N_2$  atmosphere with vigorous mechanical stirring. Then, 20-mL ammonium solution was added into the reaction mixture, which resulted in black precipitate of  $Fe_3O_4$  nanoparticles. After 30 min, the nanoparticles were separated from the suspension using a permanent magnet and repeatedly washed with distilled water. Then, the nanoparticles were dried at 50°C for 4 h.

To prepare silica-coated  $Fe_3O_4$  nanoparticles, 2.5 g of  $Fe_3O_4$  nanoparticles were dispersed for 10 min in a three-necked round bottom flask with ultrasonic irradiation. One hundred and fifty milliliters of ethanol and 40 mL of ammonium solution were then added to the  $Fe_3O_4$  suspension. The mixture of ethanol and tetraethylorthosilicate (TEOS) (89.2 and 10.8 mL) was slowly added to the  $Fe_3O_4$  suspension within 8 h. Then, the  $Fe_3O_4-SiO_2$  nanocomposite was separated from the supernatant with a permanent magnet and thoroughly washed with distilled water. And then it was dried at 50°C for 12 h.  $C_{14}/SiO_2-Fe_3O_4$  nanocomposite was prepared by surface functionalization of  $Fe_3O_4-SiO_2$  nanocomposite using triethoxyoctylsilane as a silylation agent. Two grams of  $Fe_3O_4-SiO_2$  nanocomposite and 100 mL of toluene were dispersed by ultrasonic irradiation. Ten milliliter of pyridine and 2 mL of triethoxyoctylsilane were then added into the mixture solution under vigorous mechanical stirring at room temperature for 10 h. The modified  $Fe_3O_4-SiO_2$  nanocomposite was collected with a permanent magnet and washed with ethanol several times. And then it was dried at 50°C for 12 h [33].

### 2.2.2. Synthesis of $AC-Fe_3O_4$ nanocomposite

$AC-Fe_3O_4$  nanocomposite was prepared by the coprecipitation method [39,40]. First, 8 g of  $FeCl_3 \cdot 6H_2O$  and 2.5 g of  $FeCl_2 \cdot 4H_2O$  were dissolved in 400 mL of distilled water at 80°C under nitrogen atmosphere and intense mechanical stirring for 1 h. Then, 10 g of powder-type activated carbon was added into the reaction mixture and stirred for 30 min. After mixing, 25 mL of 25% ammonia solution was added into the mixture.

Finally, the formed suspension was separated with a permanent magnet and washed several times with distilled water. The  $AC-Fe_3O_4$  nanocomposite was dried at 50°C for 12 h.

## 2.3. Characterization instruments

For characterization of the functional groups on the surface of the samples, Fourier transform infrared spectroscopy (FT-IR) analysis (Tensor 27, Bruker, Germany) was performed in the range of 400–4,000  $cm^{-1}$ . To determine the crystal phase composition of the prepared samples, X-ray diffraction (XRD) was carried out at room temperature using a D8 Advance diffractometer (Bruker, Germany) with monochromatic high-intensity  $Cu K\alpha$  radiation ( $\lambda = 1.5406 \text{ \AA}$ ), the accelerating voltage of 40 kV, and the emission current of 30 mA. The Debye–Scherrer formula was used to measure the average crystalline size of the catalysts [41]. The surface morphology of both  $C_{14}/SiO_2-Fe_3O_4$  and  $AC-Fe_3O_4$  nanocomposite was examined by field emission scanning electron microscope (FE-SEM, Hitachi S4160 Japan). The point of zero charge ( $pH_{pzc}$ ) was determined to investigate the surface charge properties of the adsorbents. The  $pH_{ZPC}$  of samples was determined adopting the method previously used [42,43].

## 2.4. Adsorption experiments

Batch adsorption experiments were performed in 1,000 mL Erlenmeyer flask containing 5 mg/L U(VI) solution and 2 g of adsorbent. The flasks were shaken at 250 rpm and at specified temperature in different contact time (5–120 min). After adsorption process, the adsorbent was separated from solution with an external magnet. The concentration of U(VI) was measured using a spectrophotometric method (UV-visible Spectrometer, Cintra 6, Australia) based on the formation of colored complex with Arsenazo(III) at 665 nm [7,44]. To evaluate various parameters on the adsorption efficiency, adsorption experiments were conducted at different initial pH (2–10), initial benzamide concentration (0–60 mg/L), contact time (5–120 min), ionic strength (0.01–1.5 M), temperature (288–333 K), initial U(VI) concentration (1–30 mg/L), and adsorbent amounts (0.4–4 g/L). The equations for obtaining removal efficiency and adsorption capacity of U(VI) are shown in Table 1. All experiments were performed in duplicate or triplicate and averaged values were reported.

Table 1

All equations used in this study (The kinetics, isotherms and thermodynamics) [1,6,15,16,28,58,59]

	Kinetic models	Thermodynamic equations	Isotherm equations
Removal efficiency $\frac{C_0 - C_e}{C_0} \times 100$	Pseudo-first-order $\ln(q_e - q_t) = \ln q_e - K_1 t$	Van't Hoff $\ln(K_1) = \frac{\Delta S}{R} - \frac{\Delta G}{RT}$	Langmuir isotherm $\frac{C_e}{q_e} = \frac{1}{bq_m} + \frac{C_e}{q_m}$
Adsorption capacity $\frac{C_0 - C_e}{W} \times V$	Pseudo-second-order $\frac{t}{q_t} = \frac{1}{k_2 q_e^2} + \frac{t}{q_e}$	Distribution coefficient ( $K_d$ ) $\frac{q_e}{C_e}$	Freundlich isotherm $\log q_e = \log K_F + \frac{1}{n} \log C_e$
	Intraparticle diffusion models $q_t = K_p \times t^{0.5} + C$	Standard free energy $\Delta G^\circ = \Delta H^\circ - T\Delta S^\circ$	Separation factor ( $R_L$ ) $\frac{1}{1 + bC_0}$

Notes: Parameters:  $C_0$  and  $C_e$  is initial and equilibrium concentrations of uranium (mg/L),  $V$  is the volume of solution (L),  $W$  is the mass of adsorbent (g),  $q_e$  (mg/g),  $q_t$  (mg/g),  $k_1$  (1/min),  $k_2$  (g/mg min),  $K_L$  (L/mg),  $q_m$  (mg/g),  $K_F$  ( $\text{mg}^{1-1/n} \text{L}^{1/n} \text{g}^{-1}$ ),  $K_p$  ( $\text{mg/g min}^{-0.5}$ ),  $C_0$  (mg/g),  $\Delta S$  (J/mol K),  $\Delta H$  (kJ/mol),  $R$  (8.314 J/mol K),  $T$  (K).

### 3. Results and discussion

#### 3.1. Characterization of the adsorbent

FT-IR spectra of  $\text{Fe}_3\text{O}_4$ ,  $\text{Fe}_3\text{O}_4\text{-SiO}_2$ ,  $\text{C}_{14}/\text{SiO}_2\text{-Fe}_3\text{O}_4$ , and  $\text{AC-Fe}_3\text{O}_4$  nanocomposite are shown in Fig. 1. For the case of  $\text{Fe}_3\text{O}_4$  nanoparticles, a single absorption peak observed at  $586 \text{ cm}^{-1}$  is related to Fe–O–Fe bond vibration [45,46]. Two FT-IR spectra of  $\text{Fe}_3\text{O}_4\text{-SiO}_2$  and  $\text{C}_{14}/\text{SiO}_2\text{-Fe}_3\text{O}_4$  nanocomposite are very similar except peaks observed at 2,914, 2,201, and  $2,232 \text{ cm}^{-1}$ . The absorption peak at  $2,914 \text{ cm}^{-1}$  in the modified  $\text{Fe}_3\text{O}_4\text{-SiO}_2$  nanocomposite is approximately twice taller than that in unmodified nanocomposite.

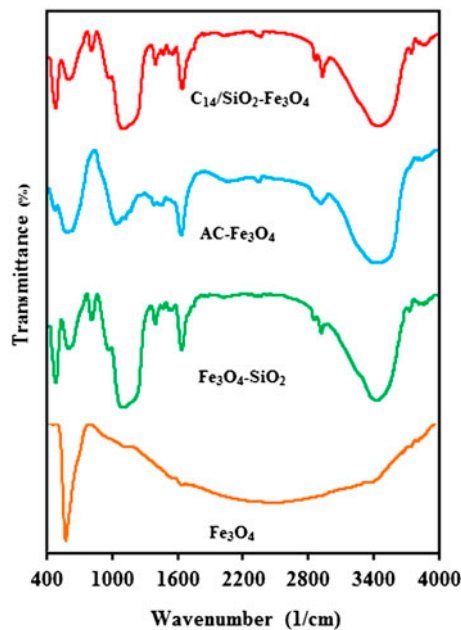


Fig. 1. FTIR spectra of the samples.

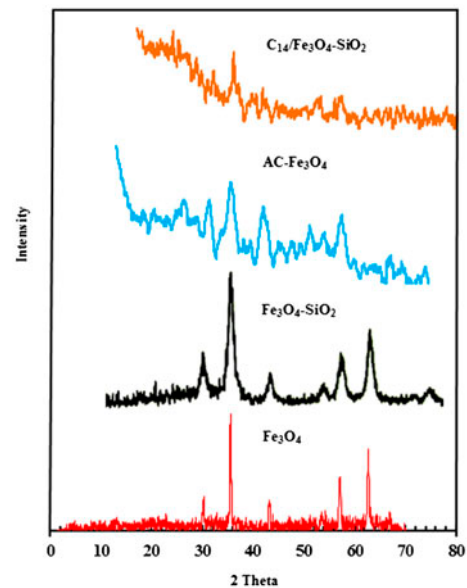


Fig. 2. XRD spectra of the samples.

This peak is related to  $\text{CH}_2$  group which originates from silane coupling agent [33]. The two peaks observed at  $2,201$  and  $2,232 \text{ cm}^{-1}$  are corresponding to  $\text{C}\equiv\text{N}$  stretching vibration [47]. This result indicates successful modification of  $\text{Fe}_3\text{O}_4\text{-SiO}_2$  by triethoxyoctylsilane. Other absorption peaks observed at  $460$  and  $800 \text{ cm}^{-1}$  in  $\text{Fe}_3\text{O}_4\text{-SiO}_2$  and  $\text{C}_{14}/\text{SiO}_2\text{-Fe}_3\text{O}_4$  nanocomposite are related to Si–O–Si stretching vibration and Si–O vibration, respectively [45]. The absorption peak at  $3,401 \text{ cm}^{-1}$  is related to O–H stretching vibration of the silanol group [35]. The band at  $1,540 \text{ cm}^{-1}$  is corresponding to asymmetric C=O stretching of carboxylate [48]. The peak at  $1,384$ ,  $1,634$ , and  $1,458 \text{ cm}^{-1}$  is attributed to the vibration of  $-\text{CH}=\text{CH}-$  double bond,

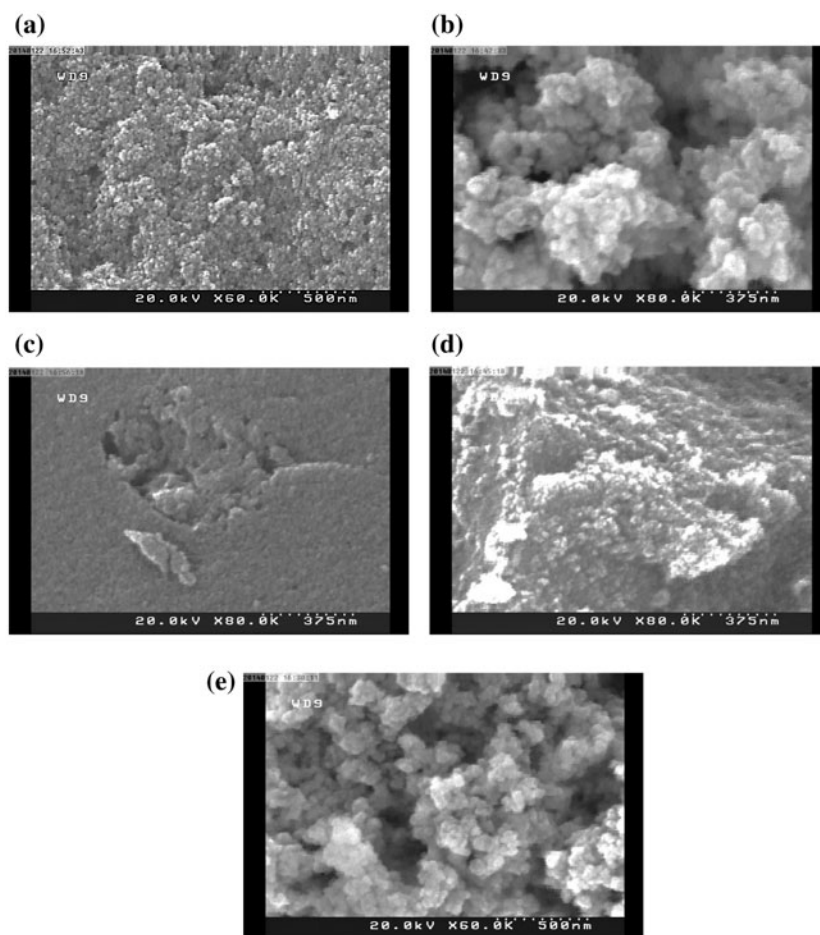


Fig. 3. SEM image of the sample: (a)  $\text{Fe}_3\text{O}_4$ , (b)  $\text{Fe}_3\text{O}_4\text{-SiO}_2$ , (c) AC, (d)  $\text{AC-Fe}_3\text{O}_4$ , and (e)  $\text{C}_{14}/\text{SiO}_2\text{-Fe}_3\text{O}_4$ .

the stretching vibrations of OH and vibrations of CH, respectively [49,50]. Also, the absorption peaks at  $3,423$  and  $1,640\text{ cm}^{-1}$  can be assigned to the adsorbed water on the silica shell or the silanol groups of the silica [32]. The absorption band at  $1,000\text{--}1,300\text{ cm}^{-1}$  of  $\text{AC-Fe}_3\text{O}_4$  nanocomposite is related to C–O stretching [51].

The crystalline structures of the  $\text{Fe}_3\text{O}_4$ ,  $\text{Fe}_3\text{O}_4\text{-SiO}_2$ ,  $\text{AC-Fe}_3\text{O}_4$ , and  $\text{C}_{14}/\text{SiO}_2\text{-Fe}_3\text{O}_4$  nanocomposite were identified by XRD analysis (Fig. 2). Diffraction peaks observed at  $30.02^\circ$ ,  $35.42^\circ$ ,  $36.62^\circ$ ,  $43.14^\circ$ ,  $57.05^\circ$ , and  $62.75^\circ$  as  $2\theta$  values were well matched with the standard patterns of  $\text{Fe}_3\text{O}_4$  [34,52]. Quite similar diffraction peaks were observed for  $\text{C}_{14}/\text{SiO}_2\text{-Fe}_3\text{O}_4$  and  $\text{AC-Fe}_3\text{O}_4$  nanocomposite, indicating the presence of crystalline phase of  $\text{Fe}_3\text{O}_4$  nanoparticles in both  $\text{C}_{14}/\text{SiO}_2\text{-Fe}_3\text{O}_4$  and  $\text{AC-Fe}_3\text{O}_4$  nanocomposite. The weak peaks appeared at low angles correspond to amorphous structure of  $\text{SiO}_2$  [35].

SEM images of  $\text{Fe}_3\text{O}_4$ ,  $\text{Fe}_3\text{O}_4\text{-SiO}_2$ , activated carbon,  $\text{AC-Fe}_3\text{O}_4$  and modified  $\text{Fe}_3\text{O}_4\text{-SiO}_2$  nanocom-

posite are shown in Fig. 3(a–e), respectively. As shown in Fig. 3(a–b) and (d–e), the morphology of nanoparticles is spherical. The SEM image in Fig. 3(a) reveals that  $\text{Fe}_3\text{O}_4$  nanoparticles have very small particle size about  $16\text{ nm}$ . Likewise, the diameter of  $\text{Fe}_3\text{O}_4\text{-SiO}_2$  nanocomposite is in the range of  $30\text{--}60\text{ nm}$  as shown in Fig. 3(b). After covering the  $\text{Fe}_3\text{O}_4$  core by silica shell, the size of  $\text{Fe}_3\text{O}_4\text{-SiO}_2$  nanocomposite is increased and the rough surface becomes smooth. Fig. 3(e) shows the morphology of  $\text{Fe}_3\text{O}_4\text{-SiO}_2$  nanocomposite after modification with triethoxyoctylsilane. The particle sizes of this nanocomposite are larger and smoother than unmodified nanocomposite. These results showed that the  $\text{Fe}_3\text{O}_4\text{-SiO}_2$  nanocomposite was completely coated by the triethoxyoctylsilane. In Fig. 3(c) and (d), it can be seen that the surface of activated carbon is completely covered by  $\text{Fe}_3\text{O}_4$  nanoparticles in size about  $20\text{--}30\text{ nm}$  after coating of  $\text{Fe}_3\text{O}_4$  on the activated carbon.

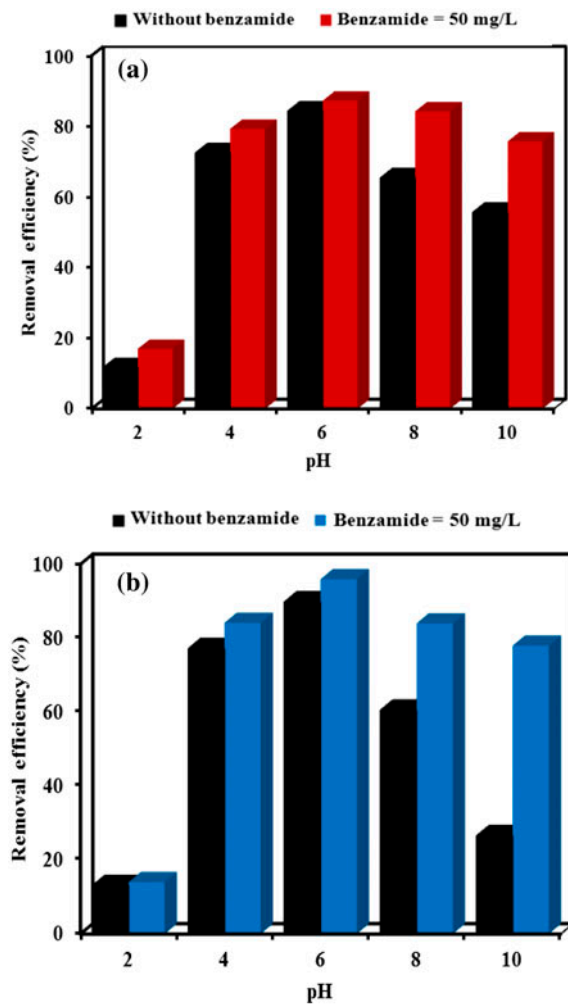


Fig. 4. Effect of pH and benzamide on the adsorption of U(VI) by (a)  $C_{14}/SiO_2-Fe_3O_4$  and (b)  $AC-Fe_3O_4$  nanocomposite (Time = 120 min,  $T = 303$  K, adsorbent dosage = 2 g/L,  $U(VI) = 5$  mg/L, benzamide = 50 mg/L).

### 3.2. The effect of operational parameters on the U(VI) removal efficiency

#### 3.2.1. The effect of solution pH

The effect of pH on the U(VI) adsorption was studied between pH 2 and 10 by 2 g/L of  $C_{14}/SiO_2-Fe_3O_4$  and  $AC-Fe_3O_4$  nanocomposite with U(VI) solutions (5 mg/L) in the presence and absence of benzamide (50 mg/L). According to Fig. 4(a) and (b), the solution pH was identified as a very important parameter in adsorption process. Removal efficiency of U(VI) by two adsorbents was increased with increasing solution pH from 2 to 6 while it was decreased above pH 6. Percentage removal of U(VI) was maximum at pH 6. It may be due to the formation of various U(VI) species and structural features of the each adsorbent at

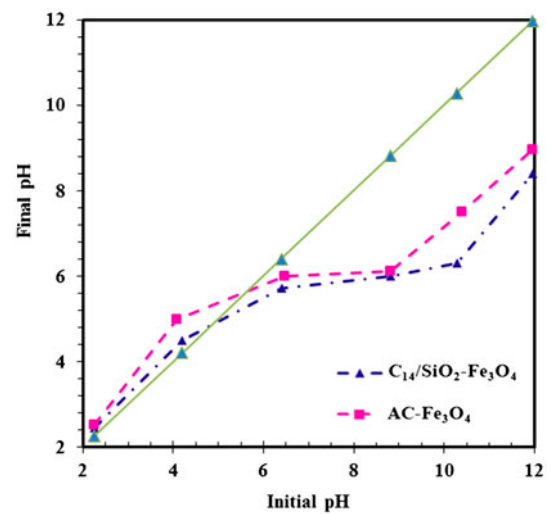


Fig. 5. The zero point charge of samples.

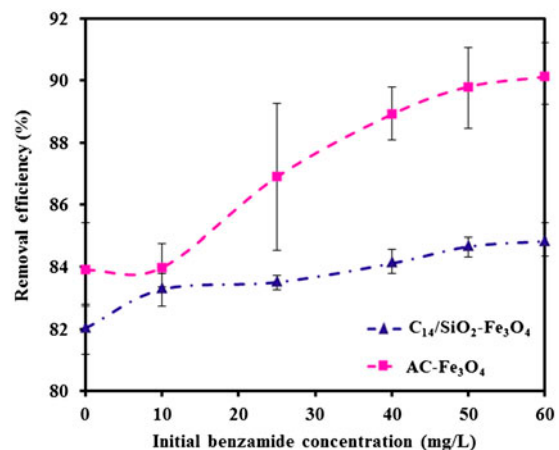


Fig. 6. Effect of initial concentration of benzamide on the adsorption of U(VI) by  $C_{14}/SiO_2-Fe_3O_4$  and  $AC-Fe_3O_4$  nanocomposite (Time = 120 min,  $T = 303$  K, adsorbent dosage = 2 g/L,  $U(VI) = 5$  mg/L).

different pHs [53]. Wang et al. reported distribution of U(VI) species in aqueous solution from pH 0–14 using a Medusa program [14]. Zero point charge of  $C_{14}/SiO_2-Fe_3O_4$  and  $AC-Fe_3O_4$  was 4.8 and 5.7, respectively (Fig. 5). In  $pH > pH_{zpc}$ , the surface is negatively charged, whereas at  $pH < pH_{zpc}$ , it is positively charged. In acidic solution, the  $UO_2^{2+}$  is a dominant U(VI) species [9,30]. Therefore, removal efficiency was very low at acidic conditions in two adsorbents because of electrostatic repulsion between protonated surface of each adsorbent and positive charges U(VI). The formation of trinuclearuranyl species began at pH 4 and was dominant at  $pH > 4.5$  [9]. Removal

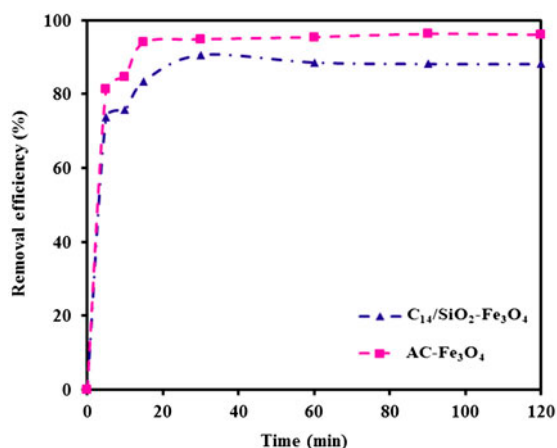


Fig. 7. Effect of contact time on the adsorption of U(VI) by  $C_{14}/SiO_2-Fe_3O_4$  and  $AC-Fe_3O_4$  nanocomposite (pH 6,  $T = 303$  K, adsorbent dosage = 2 g/L,  $U(VI) = 5$  mg/L, benzamide = 50 mg/L).

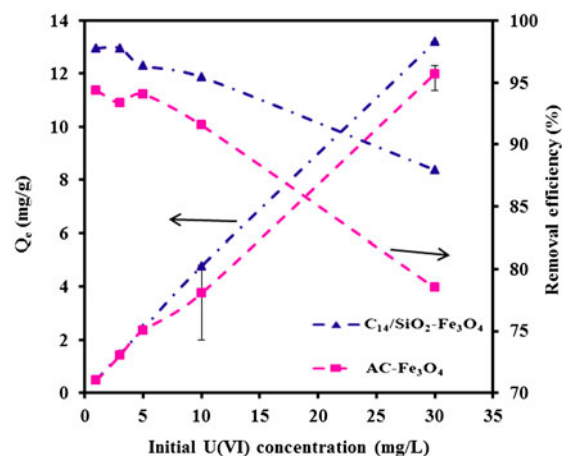


Fig. 9. Effect of initial U(VI) concentration on the adsorption of U(VI) by  $C_{14}/SiO_2-Fe_3O_4$  and  $AC-Fe_3O_4$  nanocomposite (pH 6, time = 30 min,  $T = 318$  K ( $C_{14}/SiO_2-Fe_3O_4$ ), 303 K ( $AC-Fe_3O_4$ ), adsorbent dosage = 2 g/L, benzamide = 50 mg/L).

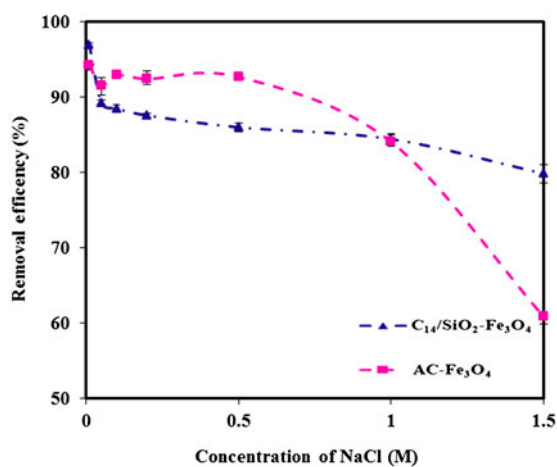


Fig. 8. Effect of ionic strength on the adsorption of U(VI) by  $C_{14}/SiO_2-Fe_3O_4$  and  $AC-Fe_3O_4$  nanocomposite (pH 6, time = 30 min,  $T = 303$  K, adsorbent dosage = 2 g/L,  $U(VI) = 5$  mg/L, benzamide = 50 mg/L).

efficiency of U(VI) reached to maximum around pH 6 because of the greatest electrostatic attraction between negative surface and positive species of U(VI). From pH > 7, the predominant U(VI) species has neutral and negative charge [24,54]. So, it can be expected that the adsorption of U(VI) become low above neutral pH. Also it could be seen from Fig. 4(a) and (b) that more positive effect of benzamide on the removal efficiency of U(VI) was observed in basic solution pH compared to that in acidic solution pH. It may be explained by the electrostatic attraction between surface of adsorbents and uranium–benzamide complex which was formed between uranium and benzamide in basic pH.

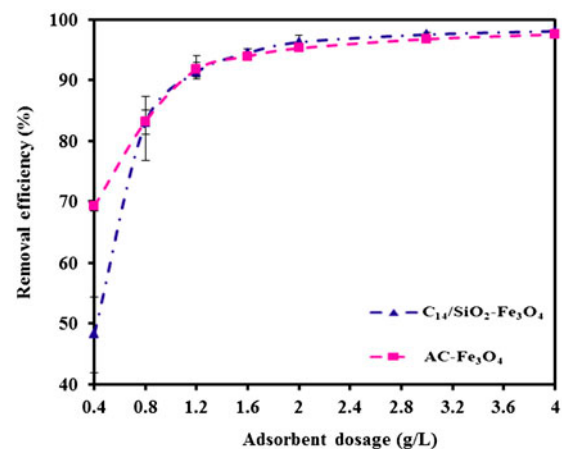


Fig. 10. Effect of adsorbent dosage on the adsorption of U(VI) by  $C_{14}/SiO_2-Fe_3O_4$  and  $AC-Fe_3O_4$  nanocomposite (pH 6, time = 30 min and  $T = 318$  K ( $C_{14}/SiO_2-Fe_3O_4$ ), 303 K ( $AC-Fe_3O_4$ ), ion strength = 0.01 M,  $U(VI) = 5$  mg/L, benzamide = 50 mg/L).

### 3.2.2. The effect of initial benzamide concentration

The effect of initial benzamide concentration on the removal efficiency of U(VI) was investigated at 5 mg/L uranium solution with variation of benzamide concentration from 0 to 60 mg/L, at 2 g/L of adsorbent and at pH 6 for 120 min. Fig. 6 indicated that the removal of U(VI) was increased in two adsorbents by adding benzamide up to 50 mg/L, but little increase was observed after 50 mg/L. The reason for the increased removal of U(VI) by adding the benzamide is related to the creation of uranium–benzamide

complex. This complex was created completely in 5 mg/L U(VI) and 50 mg/L benzamide. Similar results have been reported by other researchers [55–57].

### 3.2.3. The effect of contact time and kinetic studies

The effect of contact time on the U(VI) removal by  $C_{14}/SiO_2-Fe_3O_4$  and  $AC-Fe_3O_4$  nanocomposites was investigated with variation of reaction time from 5 to 120 min at constant concentration of U(VI) (5 mg/L), benzamide (50 mg/L) and at constant amount of adsorbent (2 g/L) at pH 6 (Fig. 7). Removal of U(VI) onto two adsorbents was quite rapid and 73.6 and 81.23% removal was observed within the first 5 min by  $C_{14}/SiO_2-Fe_3O_4$  and by  $AC-Fe_3O_4$  nanocomposite, respectively. Removal of U(VI) by  $C_{14}/SiO_2-Fe_3O_4$  nanocomposite reached to maximum in 30 min (90.58%). And the removal of U(VI) by  $AC-Fe_3O_4$  nanocomposite reached to 94.82% in 30 min. These results indicate that the adsorption of U(VI) onto two adsorbents occurred in two phase. In the first phase, adsorption occurs rapidly due to an abundant availability of active sites on the adsorbent [1,6]. Following this phase, adsorption rate is decreased and reached to an equilibrium. The reason for this trend is due to an intraparticle diffusion of U(VI) into inner surface of adsorbents and causing decrease of active sites [6,25].

The adsorption kinetic depicts valuable data about efficiency of adsorption, solute uptake rate and pathway. Adsorption kinetic experiments were performed by shaking U(VI) solution (5 mg/L) containing 2 g/L adsorbent for various contact times (5–120 min) at pH 6 and 303 K. The pseudo-first-order, pseudo-second-order and intraparticle diffusion models were chosen in order to investigate the controlling mechanism of the adsorption. The linear forms of these models are expressed in Table 1. It is obvious from Table 2 that the pseudo-second-order adsorption kinetic model has higher correlation coefficients ( $R^2$ ) in  $C_{14}/SiO_2-Fe_3O_4$  and  $AC-Fe_3O_4$  nanocomposite. Therefore, the adsorption kinetic of U(VI) onto  $C_{14}/SiO_2-Fe_3O_4$  and  $AC-Fe_3O_4$  nanocomposite was better described by the pseudo-second-order model than the pseudo-first-order and intra-particle diffusion models. These results indicate that the rate-determining step may be a chemisorption process, which involves strong interaction through sharing or exchanging of electrons between adsorbents and U(VI) [1,14].

### 3.2.4. The effect of ionic strength

The effect of ionic strength on the removal efficiency of U(VI) by  $C_{14}/SiO_2-Fe_3O_4$  and  $AC-Fe_3O_4$

nanocomposite was investigated at varying concentration of NaCl (0.01–1.5 M) at 5 mg/L U(VI), 50 mg/L benzamide and 2 g/L adsorbent at pH 6 for 30 min. The effect of ionic strength on the U(VI) removal was shown in Fig. 8. According to this Figure, the removal of U(VI) was decreased from 96.98 to 79.82% by the  $C_{14}/SiO_2-Fe_3O_4$  nanocomposite and was decreased from 94.24 to 60.82% by the  $AC-Fe_3O_4$  nanocomposite when the ionic strength increased from 0.01 to 1.5 M. A plausible reason for the decreased U(VI) removal by two adsorbents can be related to the competition between  $Na^+$  ions and U(VI) ions for the active sites of adsorbent [36,60]. According to this result, the increased ionic strength has negative effect on the removal of U(VI) by the  $C_{14}/SiO_2-Fe_3O_4$  nanocomposite. It can be related to the modification of  $Fe_3O_4-SiO_2$  nanocomposite with triethoxyoctylsilane. Other researchers also reported similar trends. For example, U(VI) removal onto carboxylate-functionalized poly (hydroxyethylmethacrylate)-grafted lignocellulosics was decreased from 99.3 to 80.6% when the ionic strength increased from 0.001 to 0.1 M [6]. Wang also reported 20% decrease in the removal of U(VI) with increasing ionic strength from 0 to 1 M [14].

### 3.2.5. The effect of temperature and adsorption thermodynamics

The effect of temperature on the removal of U(VI) was investigated at 288, 303, 318, and 333 K by contacting 2 g/L adsorbent at pH 6 for 30 min. Removal efficiency of U(VI) onto  $C_{14}/SiO_2-Fe_3O_4$  and  $AC-Fe_3O_4$  nanocomposite was increased with an increase in the reaction temperature. This indicates that the adsorption process onto  $C_{14}/SiO_2-Fe_3O_4$  and  $AC-Fe_3O_4$  nanocomposite is endothermic process. The Van't Hoff equation is expressed in Table 1. The thermodynamic parameters such as enthalpy ( $\Delta H^\circ$ ), entropy ( $\Delta S^\circ$ ) for the adsorption process were calculated from the slope and intercept of the linear plot between  $\ln K_d$  and  $1/T$ . All thermodynamic parameters are shown in Table 2. The positive value of  $\Delta H^\circ$  in Table 2 indicates endothermic nature of adsorption process. The positive value of  $\Delta S^\circ$  suggests the increased randomness at the solid/liquid interface during the adsorption of U(VI) on  $C_{14}/SiO_2-Fe_3O_4$  and  $AC-Fe_3O_4$  nanocomposite. The standard free energy values at different temperatures, those are calculated from the equation in Table 1, became negative. It demonstrates that the adsorption process of U(VI) onto  $C_{14}/SiO_2-Fe_3O_4$  and  $AC-Fe_3O_4$  nanocomposite is spontaneous. In addition, more negative values of  $\Delta G^\circ$  at higher temperature suggest that adsorption process

Table 2  
The comparison of kinetic, thermodynamic and isotherms parameters for the adsorption of U(VI)

Kinetic parameters		Pseudo-first-order		Pseudo-second-order		Intraparticle diffusion		Ref <sup>a</sup>
Adsorbent	$q_e$	$K_1$	$q_{e,cal}$	$R^2$	$K_2$	$q_{e,cal}$	$R^2$	$R^2$
Activated carbon	24.44	0.02	12.23	0.98	0.004	25.51	0.99	–
NaA zeolite	–	0.04	1.08	0.99	0.0005	2.04	0.997	0.95
Hematite	–	0.011	3.82	0.93	0.003	4.1	0.99	0.25
Natural Diatomite	–	1.18	8.28	0.63	0.04	7.99	0.66	–
HDTMA-Diatomite	–	0.68	–	0.95	0.01	–	0.97	–
Fe <sub>3</sub> O <sub>4</sub> @SiO <sub>2</sub> -AO	38.08	0.01	18.32	0.94	0.001	38.32	0.99	–
magnetic oxine	93.07	0.001	10.80	0.8059	0.004	93.46	0.9999	–
Fe <sub>3</sub> O <sub>4</sub> @TiO <sub>2</sub>	–	0.035	218.54	0.90	0.0002	101.2	0.99	–
C <sub>14</sub> /SiO <sub>2</sub> -Fe <sub>3</sub> O <sub>4</sub>	2.26	1.45	0.7644	0.66	0.54	2.22	0.9997	1.09
AC-Fe <sub>3</sub> O <sub>4</sub>	2.41	2.6	0.661	0.74	0.45	2.42	0.9999	1.21
Thermodynamic parameters		$\Delta H^\circ$	$\Delta S^\circ$	$\Delta G^\circ$ (kJ/mol)				
	$C_0$ (mg/L)	pH						
Activated carbon	100	3	(kJ/mol)	288 K	303 K	318 K	333 K	
Activated carbon <sup>a</sup>	100	4.5	–50.53	–98.76	–21.61	–19.62	–17.64	
Fe <sub>3</sub> O <sub>4</sub> @SiO <sub>2</sub> -AO	23.8	5	–46.2	–98	–16.5	–15.3	–13.6	
magnetic oxine	50	7	14.85	114.40	–	–20.38	–22.91	
Fe <sub>3</sub> O <sub>4</sub> @TiO <sub>2</sub>	–	6	39.27	141.2	–2.81	–4.22	–5.63	
C <sub>14</sub> /SiO <sub>2</sub> -Fe <sub>3</sub> O <sub>4</sub>	5	6	23.82	87.41	–1.80	–3.12	–4.86	
AC-Fe <sub>3</sub> O <sub>4</sub>	5	6	26.05	157.5	–19.34	–21.71	–24.07	
		6	23.49	149.60	–19.61	–21.86	–24.1	
Isotherm models		$q_e$ (mg/g)	Langmuir constants		Freundlich constants			
	$T$ (K)		$q_m$ (mg/g)	$b$ (L/mg)	$R^2$	$K_f^a$	$n$	$R^2$
Activated carbon	293.15	–	10.47	0.05	0.47	3.69	2.72	0.97
Activated carbon <sup>a</sup>	293.15	–	13.76	0.01	0.99	2.63	1.57	0.98
Talc	–	–	41.49	0.006	0.97	2.196	0.44	0.98
NaA zeolite	298.15	–	1.02	0.0002	0.99	0.52	6.51	0.95
Silica-coated magnetic NPs <sup>a</sup>	298.15	10	12.3	0.088	0.9	–	–	–
Hematite	293.15	–	3.36	1.01	0.99	1.56	3.84	0.89
Fe <sub>3</sub> O <sub>4</sub> @SiO <sub>2</sub> -AO	298.15	–	105	0.01	0.99	0.463 <sup>a</sup>	1.89	0.98
Fe <sub>3</sub> O <sub>4</sub> @SiO <sub>2</sub>	298.15	–	52.36	0.103	0.99	8.49	2.39	0.98
P(4-vinyl pyridine) hydrogel	303.15	–	147.06	0.47	0.98	3.15	1.93	0.97

(Continued)

Table 2 (Continued)

Isotherm models	T (K)	$q_e$ (mg/g)	Langmuir constants		Freundlich constants		[9]	
			$q_m$ (mg/g)	$b$ (L/mg)	$K_f^a$	$n$		
Natural Diatomite	294.15	–	25.63	0.03	8.11	0.16	0.82	[9]
HDTMA-Diatomite	294.15	–	667.4	0.009	45.21	0.38	0.85	[9]
magnetic oxine	298.15	–	125	0.0103	22.35	2.333	0.9040	[69]
Fe <sub>3</sub> O <sub>4</sub> @TiO <sub>2</sub>	298.15	–	91.1	0.845	33.1	0.30	0.91	[70]
Modified diatomite	298.15	–	86.78	0.0056	2.980	0.586	0.9994	[71]
C <sub>14</sub> /SiO <sub>2</sub> -Fe <sub>3</sub> O <sub>4</sub>	318	13.19	16.286	1.13	6.762	1.58	0.9792	p <sup>a</sup>
AC-Fe <sub>3</sub> O <sub>4</sub>	303	11.99	15.87	0.48	3.98	1.50	0.9731	p <sup>a</sup>

<sup>a</sup>P: Present work.

Table 3  
Separation factor  $R_L$

Initial uranium concentration (mg/L)	$R_L$ value $C_{14}/SiO_2-Fe_3O_4$	$R_L$ value $AC-Fe_3O_4$
1	0.469	0.67
3	0.227	0.4
5	0.15	0.29
10	0.081	0.17
30	0.028	0.06

of U(VI) onto two adsorbents becomes more favorable at high temperature due to a more stable bonding between U(VI) ions and active sites on the adsorbent.

### 3.2.6. The effect of initial U(VI) concentration

The effect of the initial U(VI) concentration on the adsorption capacity was studied by varying initial U(VI) concentrations (1, 3, 5, 10, and 30 mg/L) at pH 6 for 30 min (Fig. 9). At the same adsorbent doses, U(VI) removal efficiency was decreased as the initial U(VI) concentration increased. The reason for the decreased removal of U(VI) at high U(VI) concentration can be explained by the limited active sites on the adsorbent [61]. To investigate the adsorption equilibrium isotherm, experiments were performed with variation of initial concentration ranging from 1 to 30 mg/L at 2 g/L adsorbent and at pH 6 for 30 min. The Langmuir and Freundlich isotherm equations were used to fit the experimental data. The linear equations of the Langmuir and Freundlich sorption model are expressed in Table 1. The Langmuir model assumes that the removal of adsorbate occurs on an energetically homogenous surface through monolayer adsorption assuming no interactions and steric hindrance between the adsorbed molecules [62]. The basic characteristics of Langmuir isotherm can be expressed in terms of a dimensionless constant, separation factor ( $R_L$ ), which is defined in Table 1.  $R_L$  values between 0 and 1 indicate favorable adsorption, while  $R_L > 1$ ,  $R_L = 1$ , and  $R_L = 0$  indicate unfavorable, linear, and irreversible adsorption isotherm, respectively [63,64]. The Freundlich model is derived by assuming multilayer adsorption with a non-uniform distribution of adsorption heat and affinity over the heterogeneous surface [65,66]. The Langmuir and Freundlich models were analyzed by plotting  $C_e/q_e$  vs.  $C_e$  and  $\log q_e$  vs.  $\log C_e$ , respectively. Langmuir and Freundlich constants as well as related correlation coefficients are given in Table 2. The high correlation coefficients confirmed the applicability of the Langmuir isotherm for the U(VI) adsorption process onto  $C_{14}/SiO_2-Fe_3O_4$  and  $AC-Fe_3O_4$

nanocomposite. In addition, the theoretical saturated adsorption capacities of Langmuir isotherms are very close to experimental data. It suggests that monolayer adsorption is dominated in the adsorption of U(VI) onto  $C_{14}/SiO_2-Fe_3O_4$  and  $AC-Fe_3O_4$  nanocomposite. The value of  $R_L$  shown in Table 3 indicates that the adsorption process by  $C_{14}/SiO_2-Fe_3O_4$  and  $AC-Fe_3O_4$  nanocomposite is favorable. The removal capacity of  $C_{14}/SiO_2-Fe_3O_4$  and  $AC-Fe_3O_4$  nanocomposites is compared in Table 2. According to this comparison,  $C_{14}/SiO_2-Fe_3O_4$  and  $AC-Fe_3O_4$  nanocomposite has a higher adsorption capacity compared to NaA zeolite, hematite, activated carbon, and silica-coated magnetic NPs. Maximum adsorption capacity of  $C_{14}/SiO_2-Fe_3O_4$  and  $AC-Fe_3O_4$  nanocomposite was obtained as 16.29 and 15.87 mg/g at pH 6, respectively.

### 3.2.7. The effect of adsorbent dosage

The influence of adsorbent dosage on the removal efficiency of the U(VI) was tested at different amount of  $C_{14}/SiO_2-Fe_3O_4$  and  $AC-Fe_3O_4$  nanocomposite from 0.4 to 4 g/L at pH 6 for 30 min (Fig. 10). The results revealed that U(VI) removal efficiency was increased by increasing the adsorbent dosage from 0.4 to 2 g/L. The increased removal efficiency of U(VI) at higher adsorbent dosage can be attributed to the increased surface area and the availability of adsorption sites [61,67]. But as shown in Fig. 10, the removal efficiency of U(VI) was little increased beyond 1.2 g/L. According to Fig. 10,  $C_{14}/SiO_2-Fe_3O_4$  nanocomposite has more removal capacity ( $q_e = 16.29$  mg/g) for U(VI) compared to  $AC-Fe_3O_4$  nanocomposite ( $q_e = 15.87$  mg/g).

## 4. Conclusions

In the present research,  $Fe_3O_4-SiO_2$  modified with triethoxyoctylsilane and  $AC-Fe_3O_4$  nanocomposite were used as adsorbents in the removal of U(VI) with aid of benzamide as a medium agent in aqueous solutions. The prepared adsorbents were characterized

by FT-IR, XRD, and SEM analyses. The removal efficiency depended on experimental parameters like pH, contact time, ionic strength, temperature, U(VI) concentration, benzamide concentration, and adsorbent dosage. In two adsorbents, the removal efficiency was increased with increasing contact time, temperature, and adsorbent dose but was decreased with increasing ionic strength and initial U(VI) concentration. Pseudo-second-order model was better described the adsorption kinetics of U(VI) onto  $C_{14}/SiO_2-Fe_3O_4$  and  $AC-Fe_3O_4$  nanocomposites than pseudo-first-order model. The thermodynamic parameters indicated that the adsorption process by  $C_{14}/SiO_2-Fe_3O_4$  and  $AC-Fe_3O_4$  nanocomposite was endothermic and spontaneous. The high value of correlation coefficient for the Langmuir isotherms in two adsorbents suggests that adsorption occurs through homogeneous and monolayer adsorption.  $C_{14}/SiO_2-Fe_3O_4$  nanocomposite had more adsorption capacity for U(VI) (16.29 mg/g) and was less influence by increased ionic strength. This result suggests that  $C_{14}/SiO_2-Fe_3O_4$  nanocomposite is a good adsorbent for the removal of low concentration of U(VI) from aqueous solution.

### Acknowledgments

The authors would like to thank Dr Reza Davarkhah, Dr Ehsan Moradabadi, Dr Ali Esrafil, Dr Ali Maleki, DrYousef Dadban Shahamat, Mis Layla Karimi Takanlo, Mis Tayebe Abdolahi and Mr Amir Haydari for their help to carry out of this work. The financial support of this work is provided by the Tehran University of Medical Sciences and Iran radioactive Waste Management Company.

### References

- [1] Y. Tan, M. Chen, Y. Hao, High efficient removal of Pb (II) by amino-functionalized  $Fe_3O_4$  magnetic nanoparticles, *Chem. Eng. J.* 191 (2012) 104–111.
- [2] O. Ozay, S. Ekici, N. Aktas, N. Sahiner, P (4-vinyl pyridine) hydrogel use for the removal of and  $Th^{4+}$  from aqueous environments, *J. Environ. Manage.* 92 (2011) 3121–3129.
- [3] J. Li, Z. Guo, S. Zhang, X. Wang, Enrich and seal radionuclides in magnetic agarose microspheres, *Chem. Eng. J.* 172 (2011) 892–897.
- [4] A. Favre-Réguillon, G. Lebuzzit, D. Murat, J. Foos, C. Mansour, M. Draye, Selective removal of dissolved uranium in drinking water by nanofiltration, *Water Res.* 42 (2008) 1160–1166.
- [5] D. Shao, X. Wang, J. Li, Y. Huang, X. Ren, G. Hou, X. Wang, Reductive immobilization of uranium by PAAM- $FeS/Fe_3O_4$  magnetic composites, *Environ. Sci.: Water Res. Technol.* 1 (2015) 169–176.
- [6] T.S. Anirudhan, L. Divya, P.S. Suchithra, Kinetic and equilibrium characterization of uranium(VI) adsorption onto carboxylate-functionalized poly(hydroxyethylmethacrylate)-grafted lignocellulosics, *J. Environ. Manage.* 90 (2009) 549–560.
- [7] S. Sadeghi, E. Sheikhzadeh, Solid phase extraction using silica gel modified with murexide for preconcentration of uranium (VI) ions from water samples, *J. Hazard. Mater.* 163 (2009) 861–868.
- [8] Y. Zhao, J. Li, S. Zhang, X. Wang, Amidoxime-functionalized magnetic mesoporous silica for selective sorption of U(VI), *RSC Adv.* 4 (2014) 32710–32717.
- [9] M. Sprynskyy, I. Kovalchuk, B. Buszewski, The separation of uranium ions by natural and modified diatomite from aqueous solution, *J. Hazard. Mater.* 181 (2010) 700–707.
- [10] H. Parab, S. Joshi, N. Shenoy, R. Verma, A. Lali, M. Sudersana, Uranium removal from aqueous solution by coir pith: Equilibrium and kinetic studies, *Biore-sour. Technol.* 96 (2005) 1241–1248.
- [11] R. Villalobos-Rodríguez, M.E. Montero-Cabrera, H.E. Esparza-Ponce, E.F. Herrera-Peraza, M.L. Ballinas-Casarrubias, Uranium removal from water using cellulose triacetate membranes added with activated carbon, *Appl. Radiat. Isot.* 70 (2012) 872–881.
- [12] T.E. Milja, K.P. Prathish, T. Prasada Rao, Synthesis of surface imprinted nanospheres for selective removal of uranium from simulants of Sambhar salt lake and ground water, *J. Hazard. Mater.* 188 (2011) 384–390.
- [13] D. Shao, G. Hou, J. Li, T. Wen, X. Ren, X. Wang, PANI/GO as a super adsorbent for the selective adsorption of uranium(VI), *Chem. Eng. J.* 255 (2014) 604–612.
- [14] H. Wang, L. Lijian, C. Kecheng, G. Junxia, L. Jun, S. Qiang, Y. Xiaodan, L. Shoujian, Selective solid-phase extraction of uranium by salicylideneimine-functionalized hydrothermal carbon, *J. Hazard. Mater.* 229–230 (2012) 321–330.
- [15] S. Sadeghi, H. Azhdari, H. Arabi, A.Z. Moghaddam, Surface modified magnetic  $Fe_3O_4$  nanoparticles as a selective sorbent for solid phase extraction of uranyl ions from water samples, *J. Hazard. Mater.* 215–216 (2012) 208–216.
- [16] M. Schuster, K.H. Koenig, Z. Fresenius, Chromatography of metal chelates: XVIII. Influence of the coordination sites on the chromatographic properties of N, N-dialkyl-N-benzoylurea chelates, *Anal. Chem.* 331 (1988) 383–386.
- [17] M. Wazne, G.P. Korfiatis, X. Meng, Carbonate effects on hexavalent uranium adsorption by iron oxyhydroxide, *Environ. Sci. Technol.* 37 (2003) 3619–3624.
- [18] H. Bensoussan, L. Grancolas, B. Dhieux-Lestaavel, O. Delissen, C.-M. Vacher, I. Dublineau, P. Voisin, P. Gourmelon, M. Taouis, P. Lestaavel, Heavy metal uranium affects the brain cholinergic system in rat following sub-chronic and chronic exposure, *Toxicology* 261 (2009) 59–67.
- [19] J.L. Domingo, Reproductive and developmental toxicity of natural and depleted uranium: A review, *Reprod. Toxicol.* 15 (2001) 603–609.
- [20] J.D. Roach, J.H. Zapfen, Inorganic ligand-modified, colloid-enhanced ultrafiltration: A novel method for removing uranium from aqueous solution, *Water Res.* 43 (2009) 4751–4759.

- [21] M.R. Jamali, Y. Assadi, F. Shemirani, M.R.M. Hosseini, R.R. Kozani, M. Masteri-Farahani, M. Salavati-Niasari, Synthesis of salicylaldehyde-modified mesoporous silica and its application as a new sorbent for separation, preconcentration and determination of uranium by inductively coupled plasma atomic emission spectrometry, *Anal. Chim. Acta* 579 (2006) 68–73.
- [22] M.K. Sureshkumar, D. Das, M.B. Mallia, P.C. Gupta, Adsorption of uranium from aqueous solution using chitosan-tripolyphosphate (CTPP) beads, *J. Hazard. Mater.* 184 (2010) 65–72.
- [23] A. Nilchi, T. Shariati Dehaghan, S. Rasouli Garmarodi, Kinetics, isotherm and thermodynamics for uranium and thorium ions adsorption from aqueous solutions by crystalline tin oxide nanoparticles, *Desalination*. 321 (2013) 67–71.
- [24] M.A.A. Aslani, S. Yusan, N. Yenil, S. Kuzu, Sorption profile of uranium (VI) from aqueous medium onto 3-O-acetyl-(S)-1,2-O-trichloroethylidene-5,6,8-trideoxy- $\alpha$ -D-xylo-oct-5(E)-eno-1,4-furano-7-ulose (OASOTCET-DOXDXOEEFU), *Chem. Eng. J.* 200–202 (2012) 391–398.
- [25] X. Zhang, C. Jiao, J. Wang, Q. Liu, R. Li, P. Yang, M. Zhang, Removal of uranium(VI) from aqueous solutions by magnetic Schiff base: Kinetic and thermodynamic investigation, *Chem. Eng. J.* 198–199 (2012) 412–419.
- [26] S. Li, H. Bai, J. Wang, X. Jing, Q. Liu, M. Zhang, R. Chen, L. Liu, C. Jiao, In situ grown of nano-hydroxyapatite on magnetic CaAl-layered double hydroxides and its application in uranium removal, *Chem. Eng. J.* 193–194 (2012) 372–380.
- [27] A. Rahmani-Sani, A. Hosseini-Bandegharai, S.-H. Hosseini, K. Kharghani, H. Zarei, A. Rastegar, Kinetic, equilibrium and thermodynamic studies on sorption of uranium and thorium from aqueous solutions by a selective impregnated resin containing carminic acid, *J. Hazard. Mater.* 286 (2015) 152–163.
- [28] F. Ge, M.-M. Li, H. Ye, B.-X. Zhao, Effective removal of heavy metal ions  $\text{Cd}^{2+}$ ,  $\text{Zn}^{2+}$ ,  $\text{Pb}^{2+}$ ,  $\text{Cu}^{2+}$  from aqueous solution by polymer-modified magnetic nanoparticles, *J. Hazard. Mater.* 211–212 (2012) 366–372.
- [29] P. Yu, Q. Wang, X. Zhang, X. Zhang, S. Shen, Y. Wang, Development of superparamagnetic high-magnetization  $\text{C}_{18}$ -functionalized magnetic silica nanoparticles as sorbents for enrichment and determination of methylprednisolone in rat plasma by high performance liquid chromatography, *Anal. Chim. Acta* 678 (2010) 50–55.
- [30] S. Singh, K. Barick, D. Bahadur, Surface engineered magnetic nanoparticles for removal of toxic metal ions and bacterial pathogens, *J. Hazard. Mater.* 192 (2011) 1539–1547.
- [31] D. Das, M. Sureshkumar, S. Koley, N. Mithal, C. Pillai, Sorption of uranium on magnetite nanoparticles, *J. Radioanal. Nucl. Chem.* 285 (2010) 447–454.
- [32] F. Ahangaran, A. Hassanzadeh, S. Nouri, Surface modification of  $\text{Fe}_3\text{O}_4@SiO_2$  microsphere by silane coupling agent, *Int. Nano Lett.* 3 (2013) 1–5.
- [33] Y. Sha, C. Deng, B. Liu, Development of  $\text{C}_{18}$ -functionalized magnetic silica nanoparticles as sample preparation technique for the determination of ergosterol in cigarettes by microwave-assisted derivatization and gas chromatography/mass spectrometry, *J. Chromatogr. A* 1198–1199 (2008) 27–33.
- [34] J. Wang, S. Zheng, Y. Shao, J. Liu, Z. Xu, D. Zhu, Amino-functionalized  $\text{Fe}_3\text{O}_4@SiO_2$  core-shell magnetic nanomaterial as a novel adsorbent for aqueous heavy metals removal, *J. Colloid Interface Sci.* 349 (2010) 293–299.
- [35] Y.-P. Chang, C.-L. Ren, Q. Yang, Z.-Y. Zhang, L.-J. Dong, X.-G. Chen, D.-S. Xue, Preparation and characterization of hexadecyl functionalized magnetic silica nanoparticles and its application in Rhodamine 6G removal, *Appl. Surf. Sci.* 257 (2011) 8610–8616.
- [36] G. Tian, J. Geng, Y. Jin, C. Wang, S. Li, Z. Chen, H. Wang, Y. Zhao, S. Li, Sorption of uranium(VI) using oxime-grafted ordered mesoporous carbon CMK-5, *J. Hazard. Mater.* 190 (2011) 442–450.
- [37] M. Merdivan, M.Z. Düz, C. Hamamci, Sorption behaviour of uranium (VI) with N, N-dibutyl-N'-benzoylthiourea impregnated in Amberlite XAD-16, *Talanta* 55 (2001) 639–645.
- [38] F. Wang, C. Guo, L.-R. Yang, C.-Z. Liu, Magnetic mesoporous silica nanoparticles: Fabrication and their laccase immobilization performance, *Bioresour. Technol.* 101 (2010) 8931–8935.
- [39] P. He, K. Yang, W. Wang, F. Dong, L. Du, H. Liu, Nanosized  $\text{Fe}_3\text{O}_4$ -modified activated carbon for supercapacitor electrodes, *Russ. J. Electrochem.* 49 (2013) 354–358.
- [40] L.C.A. Oliveira, R.V.R.A. Rios, J.D. Fabris, V. Garg, K. Sapag, R.M. Lago, Activated carbon/iron oxide magnetic composites for the adsorption of contaminants in water, *Carbon* 40 (2002) 2177–2183.
- [41] A.L. Patterson, The Scherrer formula for X-ray particle size determination, *Phys. Rev.* 56 (1939) 978–982.
- [42] A. Mohagheghian, R. Vahidi-Kolur, M. Pourmohseni, J.-K. Yang, M. Shirzad-Siboni, Application of scallop shell- $\text{Fe}_3\text{O}_4$  nano-composite for the removal azo dye from aqueous solutions, *Water Air Soil Pollut.* 226 (2015) 1–16.
- [43] M. Shirzad-Siboni, A. Khataee, F. Vafaei, S.W. Joo, Comparative removal of two textile dyes from aqueous solution by adsorption onto marine-source waste shell: Kinetic and isotherm studies, *Korean J. Chem. Eng.* 31 (2014) 1451–1459.
- [44] Q.-H. Fan, P. Li, Y.-F. Chen, W.-S. Wu, Preparation and application of attapulgite/iron oxide magnetic composites for the removal of U(VI) from aqueous solution, *J. Hazard. Mater.* 192 (2011) 1851–1859.
- [45] H.-M. Jiang, Z.-P. Yan, Y. Zhao, X. Hu, H.-Z. Lian, Zincon-immobilized silica-coated magnetic  $\text{Fe}_3\text{O}_4$  nanoparticles for solid-phase extraction and determination of trace lead in natural and drinking waters by graphite furnace atomic absorption spectrometry, *Talanta* 94 (2012) 251–256.
- [46] Z. Zhang, J. Kong, Novel magnetic  $\text{Fe}_3\text{O}_4@C$  nanoparticles as adsorbents for removal of organic dyes from aqueous solution, *J. Hazard. Mater.* 193 (2011) 325–329.
- [47] Y. Zhao, J. Li, L. Zhao, S. Zhang, Y. Huang, X. Wu, X. Wang, Synthesis of amidoxime-functionalized  $\text{Fe}_3\text{O}_4@SiO_2$  core-shell magnetic microspheres for highly efficient sorption of U (VI), *Chem. Eng. J.* 235 (2014) 275–283.
- [48] M.R. Mauricio, H.R. de Barros, M.R. Guilherme, E. Radovanovic, A.F. Rubira, G.M. de Carvalho, Synthesis of highly hydrophilic magnetic nanoparticles of  $\text{Fe}_3\text{O}_4$  for potential use in biologic systems, *Colloids Surf., A: Physicochem. Eng. Aspects* 417 (2013) 224–229.

- [49] Y. Wei, B. Han, X. Hu, Y. Lin, X. Wang, X. Deng, Synthesis of  $\text{Fe}_3\text{O}_4$  nanoparticles and their magnetic properties, *Procedia Eng.* 27 (2012) 632–637.
- [50] H. Meng, Z. Zhang, F. Zhao, T. Qiu, J. Yang, Orthogonal optimization design for preparation of  $\text{Fe}_3\text{O}_4$  nanoparticles via chemical coprecipitation, *Appl. Surf. Sci.* 280 (2013) 679–685.
- [51] D. Mohan, A. Sarswat, V.K. Singh, M. Alexandre-Franco, C.U. Pittman Jr., Development of magnetic activated carbon from almond shells for trinitrophenol removal from water, *Chem. Eng. J.* 172 (2011) 1111–1125.
- [52] A.M. Donia, A.A. Atia, F.I. Abouzayed, Preparation and characterization of nano-magnetic cellulose with fast kinetic properties towards the adsorption of some metal ions, *Chem. Eng. J.* 191 (2012) 22–30.
- [53] R. Han, W. Zou, Y. Wang, L. Zhu, Removal of uranium(VI) from aqueous solutions by manganese oxide coated zeolite: Discussion of adsorption isotherms and pH effect, *J. Environ. Radioact.* 93 (2007) 127–143.
- [54] M. Sprynskyy, T. Kowalkowski, H. Tutu, E.M. Cukrowska, B. Buszewski, Adsorption performance of talc for uranium removal from aqueous solution, *Chem. Eng. J.* 171 (2011) 1185–1193.
- [55] K. Venkatesan, V. Sukumaran, M. Antony, P. Vasudeva Rao, Extraction of uranium by amine, amide and benzamide grafted covalently on silica gel, *J. Radioanal. Nucl. Chem.* 260 (2004) 443–450.
- [56] Y. Zhao, C. Liu, M. Feng, Z. Chen, S. Li, G. Tian, L. Wang, J. Huang, S. Li, Solid phase extraction of uranium(VI) onto benzoylthiourea-anchored activated carbon, *J. Hazard. Mater.* 176 (2010) 119–124.
- [57] M. Merdivan, S. Seyhan, C. Gok, Use of benzoylthiourea immobilized on silica gel for separation and preconcentration of uranium (VI), *Microchim. Acta* 154 (2006) 109–114.
- [58] A. Afkhami, M. Saber-Tehrani, H. Bagheri, Simultaneous removal of heavy-metal ions in wastewater samples using nano-alumina modified with 2, 4-dinitrophenylhydrazine, *J. Hazard. Mater.* 181 (2010) 836–844.
- [59] H. Zhang, J. Wang, B. Zhang, Q. Liu, S. Li, H. Yan, L. Liu, Synthesis of a hydrotalcite-like compound from oil shale ash and its application in uranium removal, *Colloids Surf., A: Physicochem. Eng. Aspects* 444 (2014) 129–137.
- [60] J. Cao, K. Lam, R. Dawson, W. Liu, S. Tao, The effect of pH, ion strength and reactant content on the complexation of  $\text{Cu}^{2+}$  by various natural organic ligands from water and soil in Hong Kong, *Chemosphere* 54 (2004) 507–514.
- [61] A.A. El-Bayaa, N.A. Badawy, A.M. Gamal, I.H. Zidan, A.R. Mowafy, Purification of wet process phosphoric acid by decreasing iron and uranium using white silica sand, *J. Hazard. Mater.* 190 (2011) 324–329.
- [62] K. Foo, B. Hameed, Insights into the modeling of adsorption isotherm systems, *Chem. Eng. J.* 156 (2010) 2–10.
- [63] X. Zhang, L. Ji, J. Wang, R. Li, Q. Liu, M. Zhang, L. Liu, Removal of uranium(VI) from aqueous solutions by magnetic Mg–Al layered double hydroxide intercalated with citrate: Kinetic and thermodynamic investigation, *Colloids Surf., A: Physicochem. Eng. Aspects* 414 (2012) 220–227.
- [64] D. Nibou, S. Khemaissia, S. Amokrane, M. Barkat, S. Chegrouche, A. Mellah, Removal of  $\text{UO}_2^{2+}$  onto synthetic NaA zeolite. Characterization, equilibrium and kinetic studies, *Chem. Eng. J.* 172 (2011) 296–305.
- [65] T.S. Anirudhan, P.G. Radhakrishnan, Improved performance of a biomaterial-based cation exchanger for the adsorption of uranium(VI) from water and nuclear industry wastewater, *J. Environ. Radioact.* 100 (2009) 250–257.
- [66] X. Shuibo, Z. Chun, Z. Xinghuo, Y. Jing, Z. Xiaojian, W. Jingsong, Removal of uranium (VI) from aqueous solution by adsorption of hematite, *J. Environ. Radioact.* 100 (2009) 162–166.
- [67] F.-L. Fan, Z. Qin, J. Bai, W.-D. Rong, F.-Y. Fan, W. Tian, X.-L. Wu, Y. Wang, L. Zhao, Rapid removal of uranium from aqueous solutions using magnetic  $\text{Fe}_3\text{O}_4@SiO_2$  composite particles, *J. Environ. Radioact.* 106 (2012) 40–46.
- [68] A. Mellah, S. Chegrouche, M. Barkat, The removal of uranium(VI) from aqueous solutions onto activated carbon: Kinetic and thermodynamic investigations, *J. Colloid Interface Sci.* 296 (2006) 434–441.
- [69] L. Tan, J. Wang, Q. Liu, Y. Sun, H. Zhang, Y. Wang, X. Jing, J. Liu, D. Song, Facile preparation of oxine functionalized magnetic  $\text{Fe}_3\text{O}_4$  particles for enhanced uranium (VI) adsorption, *Colloids Surf., A: Physicochem. Eng. Aspects* 466 (2015) 85–91.
- [70] L. Tan, X. Zhang, Q. Liu, X. Jing, J. Liu, D. Song, S. Hu, L. Liu, J. Wang, Synthesis of  $\text{Fe}_3\text{O}_4@TiO_2$  core-shell magnetic composites for highly efficient sorption of uranium (VI), *Colloids Surf., A: Physicochem. Eng. Aspects* 469 (2015) 279–286.
- [71] M. Sprynskyy, T. Kowalkowski, H. Tutu, E.M. Cukrowska, B. Buszewski, Ionic liquid modified diatomite as a new effective adsorbent for uranium ions removal from aqueous solution, *Colloids Surf., A: Physicochem. Eng. Aspects* 465 (2015) 159–167.